IR Spectroelectrochemical Methods for Studying [FeFe] Hydrogenases.

Patrick Corrigan and Alexey Silakov*

Abstract

[FeFe] hydrogenases comprise an important class of H_2 evolving enzymes. Understanding the electrochemical relationships between various active and inactive states of these enzymes is instrumental in uncovering the reaction mechanisms of the complex six-iron active center of [FeFe] hydrogenases called H-cluster. Since states of the H-cluster exhibits distinct fingerprint-like spectra in the mid-IR range, IR spectroelectrochemical experiments provide a powerful methodological framework for this goal. This chapter describes protocols for performing Fourier-transform infrared (FTIR) spectroelectrochemical experiments on [FeFe] hydrogenases. Topics included experimental design, data acquisition, and data analysis.

Keywords. Fourier-Transform Infrared Spectroscopy, [FeFe] hydrogenase, Data analysis, Spectroelectrochemistry.

1. INTRODUCTION

[FeFe] hydrogenases are an important class of enzymes that catalyze the reversible reduction of protons into H_2.[1] The organo-metallic active site of [FeFe] hydrogenases is called the H-cluster. It consists of a di-iron subcluster ($[2Fe]_H$) and a $[4Fe\text{-}4S]_H$ subcluster connected via a cysteine thiol.[2, 3] A carbon monoxide and a cyanide coordinate each iron in the $[2Fe]_H$ subcluster. The two irons are bridged by an azadithiolate and, in most states, by a μ-CO.[4–6] The $[4Fe4S]_H$ subcluster

resembles a typical four-iron ferredoxin cluster coordinated by four Cys ligands. The catalytic mechanism of the H-cluster is under debate; however, the states commonly trapped in steady-state and in potential-jump experiments, H_{ox}, H_{red}, $H_{red}H^+$, H_{sred}, and $H_{hyd}H^+$, are believed to be a part of the catalytic cycle.[7–12] The H-cluster can also be reversibly inhibited by carbon monoxide or sulfide, resulting in two distinct states called H_{ox}-CO and H_{inact} (or H_{ox}^{air}), respectively.[3, 8, 11, 13] Furthermore, in the case of the [FeFe] hydrogenase from *Clostridium beijerinckii* (*Cb*HydA1), a different H_{inact} state can be obtained that does not contain a sulfide.[11] The chemical and catalytic competence of any of the postulated active states has not been conclusively proven due to the ultra-fast nature of the catalytic processes. However, uninhibited [FeFe] hydrogenases are always under turnover conditions in aqueous solutions. Therefore, it is highly likely that the steady states observed in *in vitro* experiments are a part of the catalytic cycle and represent states preceding kinetic bottlenecks of the reaction (e.g., H^+ transfer to or from the active site, H_2 binding or leaving, etc.). [9, 12]

In the case of [FeFe] hydrogenases, Fourier-Transform IR spectroscopy is one of the most widely used spectroscopic methods. The carbon monoxide and cyanide ligands of the $[2Fe]_H$ subcluster exhibit well-defined C-O/C-N stretch vibrations between 1750 cm^{-1} and 2120 cm^{-1}. Notably, this range is free of interfering signals such as protein amide bands and water absorption.[7, 8] CN-stretching vibrations typically occupy the high-wavenumber range above 2030 cm^{-1}; terminal CO ligands exhibit C-O stretching vibrations between 1880 cm^{-1} and 2020 cm^{-1}, and μ-CO exhibit IR signals in the low-wavenumber range below 1850 cm^{-1}.

Furthermore, the frequencies of such vibrations are susceptible to the electronic environment of the corresponding ligands. In general, states of the H-cluster with a higher oxidation state of the iron ions of the $[2Fe]_H$ subcluster exhibit a higher average frequency of the terminal CO and CN bands. It is also worth noting that the CO/CN stretch-vibration frequencies depend on the electronic environment of the $[4Fe4S]_H$ cluster. In the recent publications by Senger et al., it was shown that protonation of the $[4Fe4S]_H$ cluster led to a shift of the CO/CN IR bands by about 5-7 cm^{-1}.[14] Also, in a separate publication by Rodriguez-Macia et al., redox transitions of the accessory clusters ≤10 Å away cause a small (~1 cm^{-1}) shift in the terminal CO bands, which can definitively be detected in FTIR spectra due to the narrowness of the IR bands.[15]

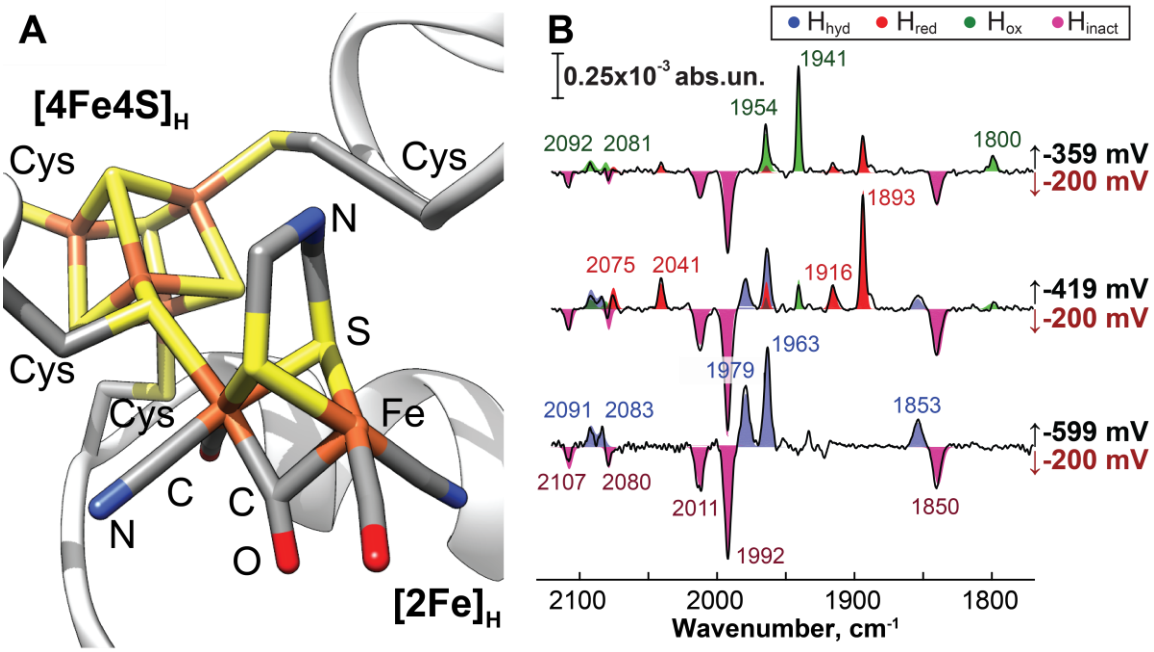

Figure 1. (A) Structure of the H-cluster in the H_{ox} state (based on crystallographic data PDB ID: 6TTL) (B) Representative difference spectra obtained during IR spectroelectrochemical experiments on *Cb*HydA1 at pH 7.4 at 10°C.

61 As the estimated turnover time of the [FeFe] hydrogenases is on the order of 10-
62 100 μs,[12] trapping and investigating intermediates of the reaction is challenging.
63 Trapping states of the H-cluster precluding rate-limiting steps is an alternative way
64 of probing the catalytic properties of these enzymes. The application of an
65 electrochemical bias is a convenient way to affect the catalysis and the oxidation
66 state of the enzyme as a whole. In conjunction with pH titrations,
67 spectroelectrochemical experiments are thus instrumental in understanding [FeFe]
68 hydrogenases. In our recent study of *Cb*HydA1, we followed three sequential
69 reduction/oxidation processes that were completely reversible using FTIR
70 spectroelectrochemical experiments.[11] These experiments highlighted the
71 staggering efficiency of reversible oxidative inactivation processes involved in the
72 mechanisms associated with an unprecedented O_2-tolerance of *Cb*HydA1.
73 Furthermore, in our IR spectroelectrocehmical experiments, we observed the H_{hyd}
74 state, which is typically only accessible under low pH and high H_2 pressures or via
75 genetic modification of the protein. Our observation in wild-type enzyme at neutral
76 pH indicated structural divergence of the protein environment of the H-cluster of
77 *Cb*HydA1 from other known species. This conclusion was later confirmed by a
78 crystallographic investigation by Winkler et al.[2]

79 Depending on the spectroscopic method of detection, spectroelectrochemical cell
80 designs vary dramatically. In case of FTIR spectroelectrochemical experiments,
81 two primary experimental methodologies exist: a protein solution transmission cell
82 or a surface absorbed protein IR cell. The latter takes advantage of the IR surface
83 enhancement effect in thin gold films (e.g. surface enhanced IR absorption,

84 SEIRA).[16] SEIRA-based experiments are advantageous due to the ability to
85 exchange solutions above the surface-absorbed protein. Unfortunately, however,
86 such a methodology is challenging to execute as one needs to create a thin gold
87 film of well-defined thickness and covalently link protein to it. In this work, we focus
88 on the transmission-cell electrochemical methodology. It is relatively simple to set
89 up, requires minimal instrumentation investment, and can be done without
90 significant modifications to a typical FTIR spectrometer. Our cell design is inspired
91 by the work of Moss *et al*[17], which shows the possibility of using a
92 semitransparent gold mesh as a working electrode to allow for IR transmission.
93 We take advantage of the resin 3D printing technology to simplify the design and
94 eliminate potential failure points, such as the possibility of breaking the connection
95 to the working electrode during the experiment, breaking CaF_2 windows during the
96 assembly, disconnecting the reference electrode from the cell due to bubble
97 formation, etc. The cell is also made to maintain an anaerobic environment and
98 can be attached to a cold plate to control the temperature. Our construction allows
99 us to achieve relatively fast cell-equilibration times and affords reproducible results
100 while maintaining an anaerobic environment outside anaerobic chambers. While
101 the protocol presented below is intended for [FeFe] hydrogenases, it can be
102 adapted to other enzymatic systems with minimal modifications.

103 **2. MATERIALS**

104 **Fabrication of the spectroelectrochemical cell.**

105 The cell was designed in Autodesk Fusion 360®. The body of the
106 spectroelectrochemical cell[18] is 3D printed using an SLA (stereolithography

apparatus) UV-curable resin printer. For this purpose, the designed cell was exported into an STL format. Using the STL file as input, we prepare the print file in ChituBox slicing software. After the print, the cell is cleaned in an isopropyl alcohol bath and cured under ultraviolet light at 395 nm. Then platinum foil with an attached copper wire lead is permanently incased into the designated niche on the sidewall of the cell using a two-part epoxy and left to cure overnight. Similarly, a gold pad that connects the gold mesh working electrode to the potentiostat lead is attached to the cell. We use a conductive temperature-harden epoxy to connect the copper leads to platinum and gold foil before the installation into the cell. To the other end of the copper leads, we solder brass pins and glued them to the cell's body with two-part epoxy (see figure 2B). The rest of the electrochemical cell is assembled at the time of sample preparation according to the schematic shown in figure 2. The cell is designed to fill the voids around the working electrode with an blank electrolyte after the cell assembly using designated ports at the top and the bottom of the cell. In our experience, the protein solution in contact with the gold mesh is not diluted by the electrolyte. We recommend printing the cell in a semitransparent resin to see any trapped bubbles while filling the cell voids with electrolyte. The aluminum plates (see figure 2C) that clamp the cell together are machined to have internal waterways for cooling and have an attachment for mounting the cell to the spectrometer's standard cell stand.

1. UV-curable resin, e.g. Siraya Tech Blu.
2. SLA 3D printer, e.g. Elegoo Mars.
3. Gold foil, 0.127mm thickness, Sigma-Aldrich.

4. Gold mesh, 0.008 mm thickness, 88.6% transparency, Precision Eforming.
5. Platinum foil, 0.25 mm thickness, Sigma-Aldrich.
6. Conductive heat-cured 1-part epoxy, e.g., Silver-bond 4 from Epoxy International.
7. Silicone sheets of 1 mm thickness to make rings and gaskets.
8. Copper wire, e.g. insulated AWG28
9. CaF_2 windows, 20 mm x 2 mm and 32 mm x 3 mm (Crystran)
10. Silicone O-rings 1/4" ID and 1/2" ID (Parker S1138 series 2-010 and 2-112, respectively).
11. BASI Ag/AgCl 3M NaCl reference electrode (MF-2052) in a 7.5 cm long, 6 mm OD glass body. Note that the cell is designed for the dimensions of this particular electrode. The use of a different electrode may require adjustments to the cell design.
12. Miscellaneous aluminum and brass stock to machine brass pins and aluminum plates.

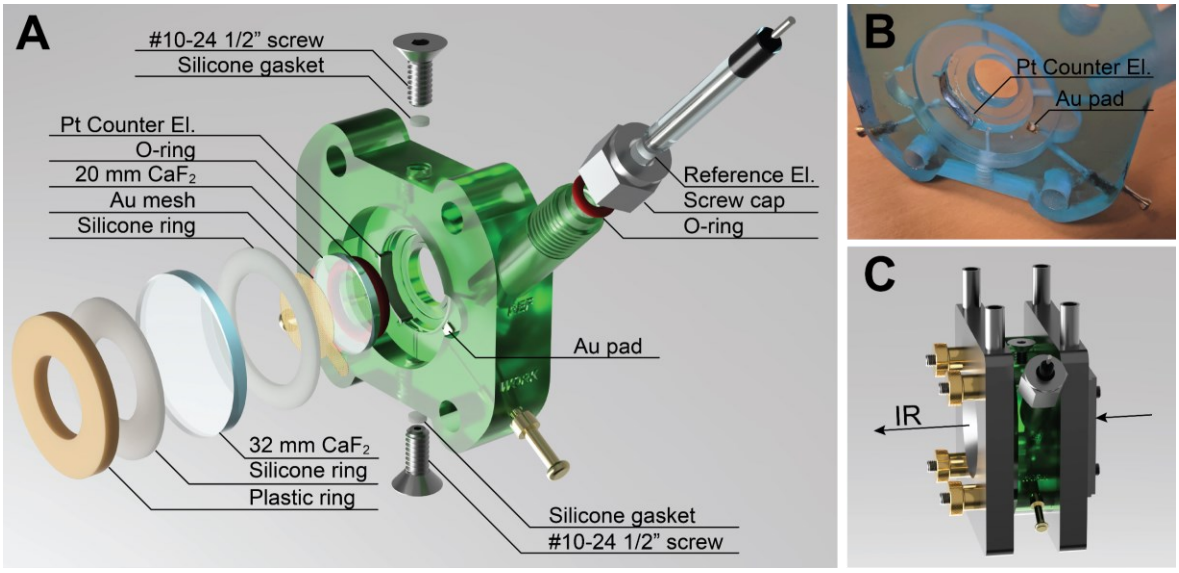

146 **Figure 2.** (A) 3D rendering of the IR spectroelectrochemical cell. (B) A photograph
147 of the SLA-printed cell's body with the installed platinum counter electrode and the
148 gold connecting pad. (C) 3D rendering of a fully assembled cell.

149

150 **Protein expression and isolation**

151 We use T7 expression strain of *E.coli* such as BL21(DE3) or a derivative thereof
152 (e.g. BL21(DE3) Δ*iscR*). In our experience, the best results are obtained if the gene
153 is fused with a cleavable N-terminus SUMO and a His_6-tag in a pET-based vector.
154 We further fuse the gene with a C-terminus strep-Tag that aids final purification
155 after cleaving the SUMO-His_6 tag. The cells are first grown aerobically in conical
156 flasks and then induced anaerobically.

157 1. Appropriate antibiotics for selective growth media (typically kanamycin).
158 2. Appropriate inducer (typically IPTG).
159 3. LB broth supplemented with 0.1M MOPS pH 7.4.
160 4. Temperature controlled shaker for 2000 mL bottles and 6L conical (e.g. New
161 Brunswick Excella E25).
162 5. 6L Elmermyer flasks (VWR).
163 6. Refrigerated centrifuge for cell pelleting and protein concentration with
164 appropriate rotors, e.g Thermo Fischer Scientific Sorvall LYNX 4000.
165 7. Sonicator as a cell lysis system, e.g. Cole-Parmer® 750-Watt Ultrasonic
166 Homogenizer.
167 8. Lysis buffer (50mM HEPES pH 7.5, 300 mM KCl, 5 mM imidazole, 10 mM
168 ß-mercaptoethanol).
169 9. Gravity-flow affinity chromatography columns.

170 10. Immobilized metal affinity chromatography (IMAC) nickel resin.
171 11. ULP1 protease. e.g. Invitrogen™ SUMO Protease.
172 12. Digestion buffer (50mM HEPES pH 7.5, 300 mM KCl, 10% (v/v) glycerol, 5
173 mM DTT)
174 13. Step-Tactin® Superflow high capacity resin (IBA GmbH)
175 14. Appropriate wash and elution buffers for affinity chromatography prepared
176 per resin manufacturer specifications.
177 15. PD-10 Desalting Columns.
178 16. SDS-PAGE system and appropriate reagents.
179 17. Bradford assay system.

180 **Protein activation**

181 Even though [4Fe4S] clusters of isolated *Cb*HydA1 appear to be mostly intact after
182 purification, we reconstitute the FeS clusters by a standard Fe and S reconstitution
183 protocol to maximize the yield of fully active protein.[11, 19] Furthermore, in our
184 protocols, the [FeFe] hydrogenase is expressed in an inactive form as we omit co-
185 expression of maturation factors responsible for the biosynthesis of the active site.
186 Therefore, the enzyme's active metallocofactor must be reconstituted as well. After
187 removing excess Fe and S with a PD10 desalting column, we add a synthesized
188 $Fe_2S_2CN_2CO_4(CH_3)NH$ cluster (synthon) to the protein solution and incubate it on
189 ice overnight under reducing conditions. Afterward, we remove the excess synthon
190 and reductant by two iterations of a PD-10 desalting column. The resulting protein
191 is mostly in the oxidized CO-inhibited state and thus must be further activated by
192 incubating under 1 atm H_2 gas for about two hours at 4ºC. Note that the H_2

193 incubation time may vary from one species of [FeFe] hydrogenase to another. The
194 resulting protein typically exhibits a mixture of the H_{ox} and the $H_{red}H^+$ states, as can
195 be verified by a transmission FTIR measurement. If the protein sample is planned
196 to be stored in cryogenic storage, we add 5-10% glycerol (or sucrose) by volume
197 to the protein solution before freezing. All above manipulations are performed
198 under strict anaerobic conditions in an anaerobic chamber.

199 1. Anaerobic chamber, e.g., a Coy Glove Box.
200 2. Fe/S reconstitution buffer, 100 mM HEPES, pH 7.5, 5 mM DTT, 500 mM
201 KCl.
202 3. FeCl3•6H2O (Sigma Aldrich).
203 4. Na2S•9H2O (Sigma Aldrich).
204 5. Synthesized $Fe_2S_2CN_2CO_4(CH_3)NH$, synthesis protocols can be found
205 elsewhere.[20–22]
206 6. H-cluster reconstitution buffer, 25 mM TAPS pH 8.0, 100mM KCl , 5mM
207 NaDT.
208 7. Appropriate electrochemical buffers.
209 8. Store small aliquots of proteins in cryovials at -20° C.

210 **Infrared spectrometry and electrochemistry**

211 1. FTIR spectrometer, e.g. Thermo Scientific Nicolet is50 FTIR equipped with
212 an MCT-A LN_2-cooled detector.
213 2. A 3.6 µm long-pass visible light filter, e.g. Edmund Optics, to block
214 irradiation from the internal aligning red laser that may cause photo-induced
215 reactions in [FeFe] hydrogeanses.

216 3. Recirculating chiller (VWR) for temperature control.
217 4. Liquid nitrogen for cooling the MCT-A detector.
218 5. Supply of dry nitrogen gas for removing water vapors from the IR
219 spectrometer and the sample chamber.
220 6. Potentiostat, e.g. Pine research WaveNow.

221 **3. METHODS**

222 **IR cell assembly**

223 1. A 20 mm OD CaF_2 window is placed on top of an appropriate O-ring at the
224 bottom of the cell.
225 2. Gold mesh is carefully placed and aligned so that one of the corners is on
226 top of the gold pad. We achieve the best results if the gold mesh is cut into
227 a teardrop shape.
228 3. A 1 mm silicone spacer ring is placed by pressing down the gold mesh to
229 the gold pad. Depending on the roughness of the 3D printed cell surface, a
230 small amount of silicone vacuum grease may be added to the ring on both
231 sides to ensure an air-tight seal of the cell. However, we recommend
232 polishing the mating cell surface instead and not using any grease.
233 4. Any liquid from the storage solution of the gold mesh is removed by gently
234 pressing a kim-wipe to the surface.
235 5. About 15 μL of the sample solution is placed in the middle of the mesh,
236 preferably in one drop, to avoid bubbles.

237 6. A 32 mm CaF_2 window is gently placed on top. It is important to place this
238 window as straight as possible to avoid pushing protein liquid to one side of
239 the cell.
240 7. Another 1 mm silicon spacer is placed onto the upper CaF_2 window and
241 followed by a plastic ring.
242 8. The whole assembly is then placed on a custom-made aluminum plate and
243 capped by another.
244 9. Four thumb nuts are screwed in place to clamp the assembly together. Nuts
245 have to be tightened gently in a crisscross pattern until the gold mesh
246 noticeably flattens and the protein liquid is evenly distributed over the visible
247 space of the cell.
248 10. Inject electrolyte prepared anaerobically through the lower port using a gas-
249 tight syringe, penetrating the silicone gasket until all voids in the cell
250 between all three electrodes are filled, and the liquid starts filling the port of
251 the reference electrode. Keep the upper filling port open to avoid trapping
252 bubbles that would electrically disconnect the reference electrode from the
253 rest of the cell.
254 11. Once the electrolyte fills up the port of the reference electrode, the reference
255 electrode is secured in place by an o-ring and a stainless steel yor-loc nut
256 for 1/4"-OD tube.
257 12. At this time, upper and lower filling ports are sealed by tightening the
258 corresponding #10-24 stainless-steel screws.

13. It is also important to check the resistance between the counter electrode and the reference electrode. In our experience, the resistance is typically 100-200 kOhm. We advise against measuring the resistance between the working electrode and other electrodes as the potential applied by a multimeter while taking a resistance measurement may irreversibly damage protein.

IR Spectroelectrochemical measurements

We typically perform experiments on [FeFe] hydrogenase at 10° C using 0.25-1.0 mM protein solution. FTIR spectra are recorded at 2 cm^{-1} resolution with 500 scans per spectrum using Thermo Scientific™ OMNIC™ Series Software. For the flexibility of post-processing, data is recorded in the "Single Beam" mode, which is then converted to the absorbance spectrum during data processing (see below).

1. Prior measurements, calibrate the reference Ag/AgCl electrode by measuring cyclic voltammetry of a methyl viologen solution using a standard electrochemical cell. Typically, methyl viologen mid-point potential reads about -640 mV – -650 mV vs Ag/AgCl. The actual Ag/AgCl electrode potential can be then calculated using the known value of $E_0(MV^{2+}/MV^{\cdot+})$ = -446 mV vs NHE.[23]
2. Assemble the cell with a buffer identical to that of the protein sample. Measure a background IR spectrum using the same settings as those to be used for spectroelectrochemical measurement. Since the cell's path length is dependent on the pressure imposed by the thumbscrews, the cell assembly must be done with the same care as that for the actual

282 experiment. For the best result, accumulate the background with at least
283 double the number of scans used in the actual experiment to avoid a
284 reduction in the signal-to-noise ratio during data processing.

285 3. If needed, thaw protein, adjust the buffer to the appropriate pH and ensure
286 that the protein solution contains at least 100 mM of KCl (or NaCl).

287 4. Assemble the cell with the protein solution, place it in the spectrometer and
288 connect the potentiostat's leads to the cell.

289 5. Connect the water cooling tubes to the IR cell, turn on the chiller at the
290 desired temperature, and after ~15 minutes, verify the actual temperature
291 of the cell by a thermocouple or an IR thermometer. Adjust set temperature
292 at the chiller if needed.

293 6. Once the cell's temperature is equilibrated, record a control IR spectrum to
294 verify the quality of the sample. At this point, the composition of states in
295 the [FeFe] hydrogenase should be similar to that of the as-activated sample
296 in a regular transmission IR cell. This spectrum can also be used as a
297 background spectrum during data processing for generating differential IR
298 spectra. If so desired, this spectrum must be accumulated to a higher quality
299 than the actual spectroelectrochemical data to avoid degradation of the
300 signal-to-noise ratio upon data processing.

301 7. Create a macro that allows repeated accumulation of the IR spectra. The
302 delay before each measurement should allow for a sufficient cell/protein
303 equilibration upon a potential step (5-10 min).

8. Setup sequential potential-step chronoamperometry (CA) measurements in the potentiostat's software. The total duration of each CA experiment must match the repetition time of the IR measurements exactly.
9. In our experience, the initial step from an "open-cell" to the most negative potential requires about 15 min of equilibration. Therefore, we recommend that the initial potential setting be done manually before initiating the spectroelectrochemical experiment.
10. Execute both the IR macro and CA experiments as synchronously as possible.
11. Make sure that the cell's current does indeed stabilize within the designated equilibration time. Every sequential step of ±15-25 mV results in an almost instantaneous current equilibration. However, we recommend including a 5 min equilibration time for each potential step to ensure protein is in equilibrium with the working electrode.
12. After completing the experiment, perform another calibration of the Ag/AgCl reference electrode using the same methodology as in step 1 to ensure that the reference electrode potential was stable during the experiments. If a significant deviation is observed, use time stamps for each IR measurement to interpolate the reference potential drift based on the "before" and "after" values.

Data processing.

The data processing methodology presented here is based on using Kazan Viewer, a toolbox for MATLAB.[24] However, similar procedures can be performed

using other scientific software and, in some cases, by the software that controls the spectrometer (e.g. Omnic). Here we give an example of the workflow.

1. Load the software.
    - Open MATLAB. If Kazan viewer is properly installed, execute "kazan" command to load the software. If it is not yet installed, download the software,[24] unpack the zip file and then add the path to the "viewer" folder in the MATLAB environment.
2. Load the background and the absorption spectra into the software to generate an absorbance spectrum.
    - Open the "ftirbox" plugin in Kazan Viewer. Load the background spectrum to Kazan viewer (for Omnic-generated data, choose "*.spa" then "NicoletSPA" and at the bottom "Absorbation/Transmission") and use "Set baseline" in the FTIR box (also mark "use BL"). Load an experimental spectrum to Kazan viewer and click "Set Data" in the FTIR box.
3. Model the baseline of the experimental spectrum and subtract it.
    - In the FTIR plugin, change the setting from "Polynomial" to "Cubic spline" under the baseline portion of the plugin window. Unmark "Point Based" to set baseline points to be based on the experimental data points. Add baseline points by clicking the "Add" button under "baseline" to add baseline points. Every mouse click will add a baseline point to memory (nothing will be displayed). Press Enter on the keyboard to exit adding mode and display added points. Adjust

positions of the baseline points until the baseline reproduces well the experimental background. FTIR box automatically generates a difference which can be used to verify the baseline correction process if Kazan viewer is set for the two-axis visualization mode ("Re/Im" button).

4. Save the obtained absorbance spectrum.
    - In Kazan viewer, transfer the result of the baseline fit from the plugin buffer (Output) to that of Kazan viewer (Source) by clicking the "≪" button and selecting "FittDiff" in the appeared window. Then click "Save Source" in the "File" menu to save the file.
5. Write down the intensity of the bands most representative of specific states.
6. Repeat steps 2-5 for each IR data set obtained.
7. Plot the intensity of the relevant IR bands as a function of applied potential.

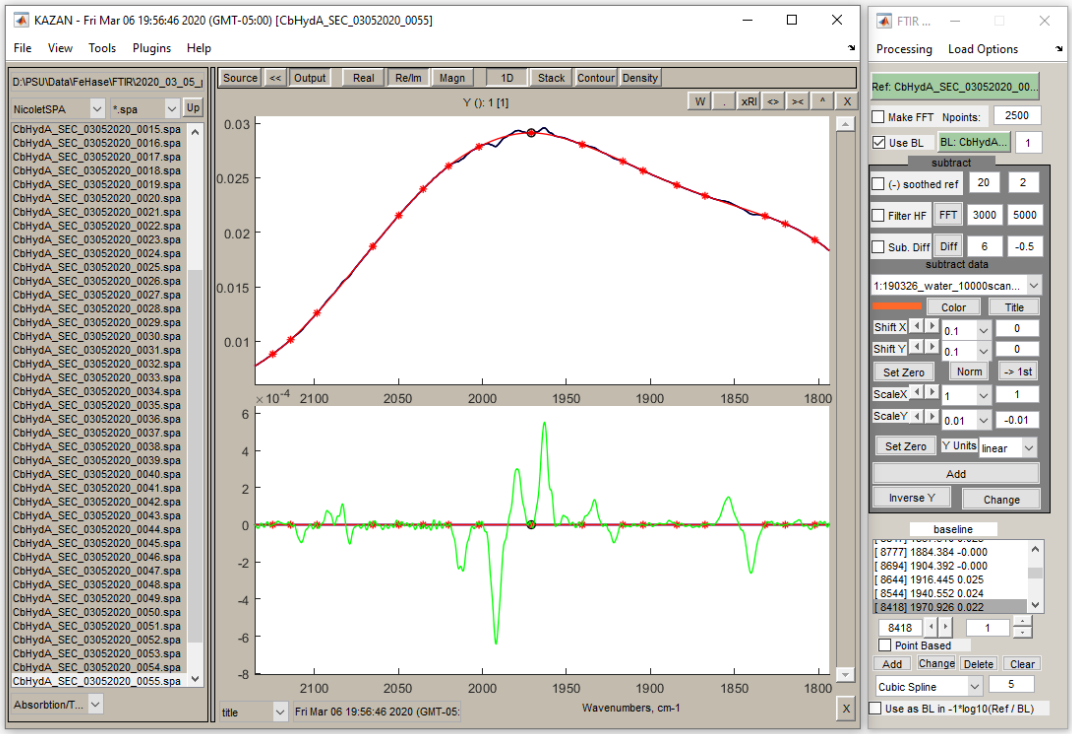

Figure 3. Example of data processing using Kazan Viewer and the FTIR Box plugin. Black trace - absorbance data obtained by calculating $A = \log_{10}\left(\frac{Ref}{BL}\right)$, where Ref is the spectrum of *Cb*HydA1 obtained at -609 mV and BL is the "baseline" spectrum of *Cb*HydA1 obtained at -200 mV, Red trace - simulated baseline generated as a Cubic spine of preselected data points (shown as red asterisks), Green traces – baseline subtracted spectrum, Orange trace - additional data to be subtracted (e.g., water vapor spectrum), in the case shown the scale factor is set to zero.

Data analysis

Midpoints potentials for the redox transitions between various states can be extracted by fitting the potential dependence of the absorbances to the Nernstian equation: $\frac{C_{red}}{C_{ox}} = \exp\left(-\frac{nF}{RT}\,(E - E_0)\right)$ (1)

where C_{red}, C_{ox} are potential (E) dependent concentrations of reduced and oxidized species, respectively; E_0 is the redox mid-point potential; $F = 96485.33\ C\ mol^{-1}$ is the Faraday constant; $R = 8.314462\ J\ K^{-1} mol^{-1}$ is the

universal gas constant; T is temperature, and n is the number of electrons transferred. At 10°C (283.15K) $\frac{F}{RT} = 0.041\ mV^{-1}$. In the case of *Cb*HydA1, it is possible to access four states through three one-electron transitions.[11] To generalize, we will call these states A, B, C and D, where A is the most reduced and D is the most oxidized. In the case of *Cb*HydA1, A=H_{hyd}, B=H_{red}, C=H_{ox}, and D=H_{inact} and each redox transition require one electron. Consequently, to interpret the IR spectroelectrochemical data, a system of four equations must be considered:

$$\begin{cases} C_A(E) = C_B(E)S_{AB}(E) \\ C_B(E) = C_C(E)S_{BC}(E) \\ C_C(E) = C_D(E)S_{CD}(E) \\ C_A(E) + C_B(E) + C_C(E) + C_D(E) = 1 \end{cases} \quad (2)$$

where $S_{AB}(E) = \exp\left(-\frac{F}{RT}(E - E_0^{AB})\right)$, $S_{BC}(E) = \exp\left(-\frac{F}{RT}(E - E_0^{BC})\right)$, $S_{CD}(E) = \exp\left(-\frac{F}{RT}(E - E_0^{CD})\right)$, and E_0^{AB}, E_0^{BC} and E_0^{CD} are midpoint potentials for A⇋B+e^-, B⇋C+e^- and C⇋D+e^- transitions, respectively. By applying the Beer-Lambert law, it is trivial to derive the final set of equations for the potential dependence of the absorbances ($Abs_i, i \in \{A, B, C, D\}$):

$$Abs_A(E) = \ell\varepsilon_A K(E)S_{ab}(E)S_{bc}(E)S_{cd}(E) \quad (3)$$

$$Abs_B(E) = \ell\varepsilon_B K(E)S_{bc}(E)S_{cd}(E) \quad (4)$$

$$Abs_C(E) = \ell\varepsilon_C K(E)S_{cd}(E) \quad (5)$$

$$Abs_D(E) = \ell\varepsilon_D K(E) \quad (6)$$

$$K(E) = [S_{ab}(E)S_{bc}(E)S_{cd}(E) + S_{bc}(E)S_{cd}(E) + S_{cd}(E) + 1]^{-1} \quad (7)$$

Where ε_A, ε_B, ε_C, ε_D are extinction coefficients of the characteristic CO bands of states A, B, C, and D, respectively, and ℓ is the pathlength. Typically, ℓ, ε_A, ε_B, ε_C,

ε_D are not well defined and therefore are fitting parameters (ℓ can be implicitly included into $\varepsilon_i^* = \ell\varepsilon_i$).

Using the equations above, it is possible to construct a simple fitting routine. However, even for the more complex case of three one-electron transitions, a simulation by manual variation of the seven parameters ($E_0^{AB}, E_0^{BC}, E_0^{CD}, \varepsilon_A^*, \varepsilon_B^*, \varepsilon_C^*, \varepsilon_D^*$) typically provide a sufficiently accurate result. For illustration purpose, below, we provide a script for MATLAB that simulates the spectroelectrochemical traces of *Cb*HydA1 measured at pH 7.4[11] (note that this script also runs in the freely available MATLAB-like environment, Octave):

```
clear all; % ensures clean start of the script
% Experimental concentration profiles normalized to total sum:
Hhyd=[1.029,0.969,0.969,1.013,1.029,0.998,0.998,0.969,0.969,0.915,...
0.879,0.843,0.752,0.488,0.289,0.199,0.090,0,0.0,0,0,0,0,0,0,0,0,0];

Hred=[0,0,0,0,0,0,0.007,0.028,0.047,0.075,0.115,0.177,0.253,0.386,...
        0.437,0.391,0.270,0.117,0.040,0.015,0,0,0,0,0,0,0,0];

Hox=[0,0,0,0,0,0,0,0,0,0.013,0.007,0.023,0.040,0.113,0.244,0.397,...
0.536,0.485,0.288,0.179,0.118,0.077,0.062,0.044,0.035,0.026,0.015,0];

Hinact=[0,0,0,0,0,0,0,0,0,0,0,0,0,0,0.005,0.063,0.112,0.339,0.603,...
        0.772,0.865,0.913,0.948,0.948,0.979,1.005,1.005,1.];
% Applied potential mV vs NHE:
    E = -614:15:-209;
% Midpoint potentials:
    Eab = -415; % Hhyd<=>Hred
    Ebc = -392; % Hred<=>Hox
    Ecd = -359; % Hox<=>Hinact
% Constants
    T = 283.15; % K = 10deg C
    FnRT = 1*96485.33/8.314462/T*1e-3; % mV^-1
% Calculating exponential primitives:
    Sab = exp(-FnRT*(E-Eab));
    Sbc = exp(-FnRT*(E-Ebc));
    Scd = exp(-FnRT*(E-Ecd));
    K = 1./(Sab.*Sbc.*Scd+Sbc.*Scd+Scd+1);
% Calculating concentration profiles:
    D = K;
    C = K.*Scd;
    B = K.*Sbc.*Scd;
```

```
    A = K.*Sab.*Sbc.*Scd;
% Plotting results into a plot window with ID "777":
figure(777); clf; hold on;
plot(E, A, '-r', E, B, '-g',E, C, '-m', E, D, '-b');
plot(E, Hhyd, 'or', E, Hred, 'og',E, Hox, 'om', E, Hinact, 'ob');

xlabel('Potential, mV vs NHE'); ylabel('Normalized absorbance')
legend('H_{hyd}', 'H_{red}H^+', 'H_{ox}', 'H_{inact}', ...
    'Orientation', 'horizontal');
```

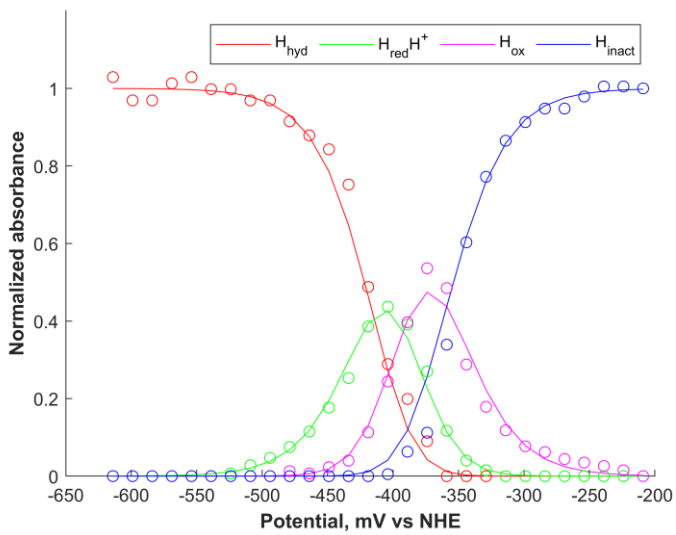

Figure 4. Example potential dependence of concentration profiles of four states observed in the spectroelectrochemical experiments on *Cb*HydA1 at pH 7.4 (circles) and the fit to the equations 3-7 accounting for 1e$^-$-transitions. The figure is generated by the script above.

4. NOTES

1. We find that [FeFe] hydrogenases interact well with the working gold electrode directly; thus, the addition of mediators does not significantly improve the cell's equilibration time, nor does it affect the experimental results. Therefore, in all our experiments, we omit using mediators altogether.[10, 11] However, we would like to note that experiments on other metalloproteins may benefit from the use of mediators. A need for mediators may be evident from a hysteretic and a non-Nernstian behavior of

426 concentration profiles with applied potentials. If that is the case, generally,
427 it is advised to choose a set of mediators so that their midpoint potentials
428 cover the whole desired range of potentials with a roughly 50-100 mV
429 spacing between closest values. Also, note that the redox potentials of
430 some mediators may have strong pH dependence, and thus an adjustment
431 to the mediator mix may be needed for different pH values. Furthermore,
432 note that some mediators' low solubility in aqueous solutions (e.g.,
433 quinones) may present an additional obstacle. A comprehensive list of
434 mediators can be found elsewhere.[25]

435 2. Since the spectroelectrochemical experiments are commonly performed at
436 lower temperatures (e.g., 10°C), it is important to note that buffers have
437 temperature-dependent drifts of the pH values. Such effects must be
438 accounted for by either making buffers at the same temperature as the
439 spectroelectrochemical experiments or adjusting the reported pH values
440 according to the known temperature dependence.

441 3. We synchronize the execution of the macro for potential step
442 chronoamperometry and the macro for the accumulation of FTIR spectra by
443 hand. However, some instruments allow setting up an electrical triggering
444 that would let the user synchronize the two devices for every potential step
445 automatically. If such an option is available, we recommend utilizing it as
446 this saves time in timing experiments and ensures no accumulated
447 "frameshift" over the 10-20-hour long experiment.

4. For data processing, we find it sometimes helpful to calculate the sum of concentrations of each state involved to find pathlength-dependent extinction coefficients. We vary the scaling factor for each concentration profile until the sum of all concentrations appears as linear as possible. Furthermore, the gradual decay of the concentration sum through the progression of the experiment is a good indication of protein degradation during the experiments. Also, one can use the total sum to verify the correctness of the electrochemical reaction model since an omission of a state from the sum would result in an irregularity in the total sum at certain potentials.
5. Baseline modeling of the IR spectra must be done with utmost care. Since the cubic spline function is a gradient-based interpolation method, it is possible to accidentally create artificial peaks or eliminate real signals if the two selected baseline points are too close to each other on a spectrum and have a significant difference in the y-value. As a rule of thumb, we place the two nearest baseline points at least 10 cm^{-1} apart.
6. Over the course of an experiment, the water vapor spectrum may change due to the changes in the atmospheric pressure or the pressure of the drying N_2 gas. As a result, data traces may contain various amounts of water vapor signals. This variation has to be accounted for during data processing. To appropriately subtract a water vapor spectrum, the water vapor signals need to be extracted from the background spectrum either by acquiring and subtracting background spectra before and after the

spectroelectrochemical experiment or by baseline-modeling the transmission (Single Beam) data of the background spectrum and calculating water-vapor absorbance spectrum using this baseline model as a background (option "Use as BL in -1*log10(Ref/BL)" in the FTIR plugin of Kazan viewer, see figure 5). Some spectrometer software has an option of atmospheric suppression; however, in our experience, this function does not provide a satisfactory result.

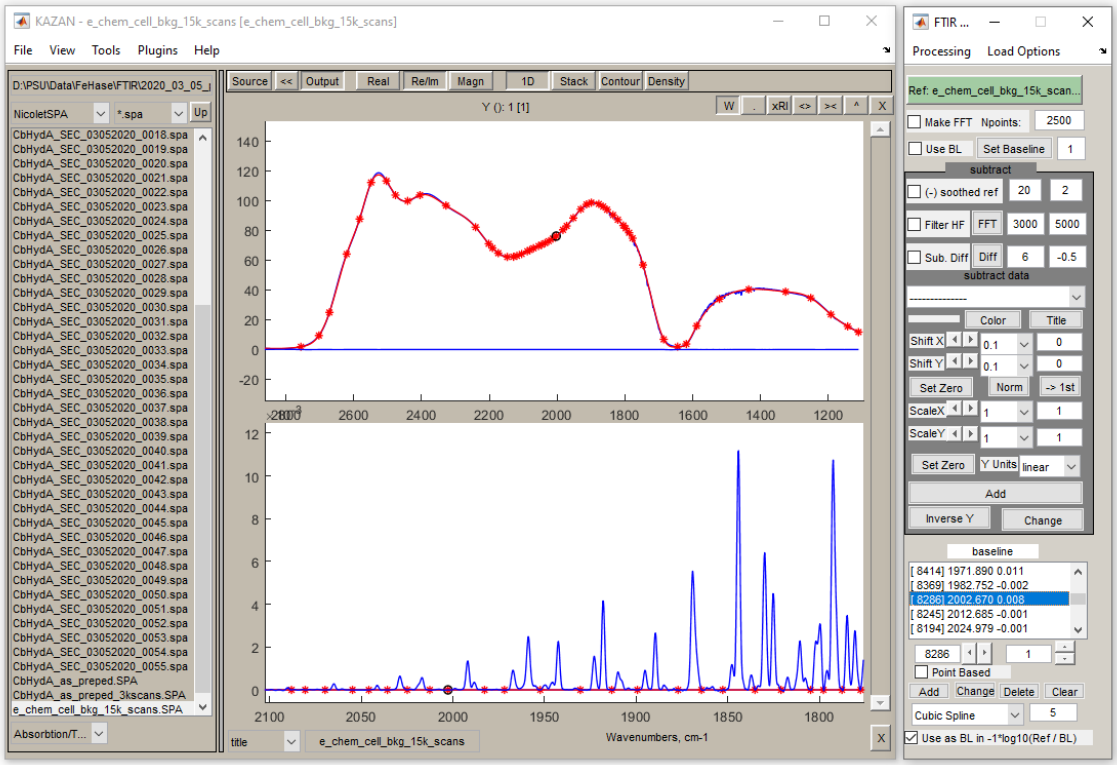

Figure 5. Example of extracting water vapor spectrum using Kazan viewer and FTIR plugin to aid data processing.

7. Manual processing of IR spectra is very time-consuming and leaves room for an implicit bias via manual background modeling (e.g., see note 5 above). An alternative possibility is to employ an automatic processing routine that minimizes the "human factor." Unfortunately, making robust

code requires considerable programming skills. Therefore, we only recommend this route if a large set of experiments need to be analyzed in a short period of time. We recommend employing the singular value decomposition (SVD) framework that can significantly simplify programming. For this method, each observed state of the H-cluster must be accurately modeled by a set of Gaussian (or Voigt) functions. The correctness of the model spectra can be verified by target testing.[26] The baseline can be represented by a set of polynomial primitives. Then the model spectra, together with the baseline polynomial primitives, can be used in a global analysis to extract potential-dependent concentration profiles. The following set of equations outlines the concept:

$$D(E,\nu) = U(E)\Sigma V(\nu)^* \tag{8}$$

$$V_{test}(\nu) = \left[\underbrace{\left(S_1(\nu)\right), \left(S_2(\nu)\right), \dots, \left(S_n(\nu)\right)}_{\substack{Model \\ spectra}} \underbrace{(\nu), (\nu^2), \dots (\nu^k)}_{\substack{polynomial \\ primitives}}, S_{water}(\nu)\right] \tag{9}$$

$$R = \frac{\Sigma V^*}{V_{test}^*} \tag{10}$$

$$U_{test}(E) = UR \tag{11}$$

where n - number of observable states (including instrumental artefacts and inhibited states), $S_i(\nu)$ – columns of modeled spectra of each observable state ($i \in \{1, 2, 3 \dots n\}$), $\left(\nu^j\right)$ - columns of power functions of wavenumber ($j \in \{1, 2, 3 \dots k\}$), k - the highest order of the polynomial, $V_{test}(\nu)$ - 2D matrix, where each column represents a spectrum or a polynomial primitive, $U_{test}(E)$ - resulting concentration profiles with each column representing the

potential dependence of each component of V_{test}. Following is a rough workflow that needs to be programmed.

- The 2D dataset $D(E, \nu)$ is truncated to the desired wavelength range (e.g., 1800 cm^{-1}- 2120 cm^{-1}).
- A singular value decomposition is performed on the truncated dataset (eq. 8).
- Each state is modeled and assembled into a 2D matrix $V_{test}(\nu)$ (eq. 9).
- $V_{test}(\nu)$ is augmented with polynomial primitives and, if necessary, by a water vapor spectrum. Note that the total number of columns $N = n + k$ must be less than or equal to the total number of experimental spectra accumulated in the 2D data set.
- The transformation matrix R is calculated according to equation 10. Note that matrixes Σ and V must be truncated to the rank of N.
- Potential dependence of all spectral components of V_{test} are calculated according to equation 11.

Acknowledgment

This material is based upon work supported by the National Science Foundation under Grant No. (CHE-1943748) and by the US Department of Energy (DESC0018087).

5. REFERENCES

530 1. Lubitz W, Ogata H, Rüdiger O, Reijerse E (2014) Hydrogenases. Chem Rev
531 114:4081–4148. https://doi.org/10.1021/cr4005814

532 2. Winkler M, Duan J, Rutz A, et al (2021) A safety cap protects hydrogenase from
533 oxygen attack. Nat Commun 12:756. https://doi.org/10.1038/s41467-020-20861-2

534 3. Esselborn J, Muraki N, Klein K, et al (2016) A structural view of synthetic cofactor
535 integration into [FeFe]-hydrogenases. Chem Sci 7:959–968.
536 https://doi.org/10.1039/c5sc03397g

537 4. Silakov A, Wenk B, Reijerse E, Lubitz W (2009) (14)N HYSCORE investigation of the
538 H-cluster of [FeFe] hydrogenase: evidence for a nitrogen in the dithiol bridge. Phys
539 Chem Chem Phys 11:6592–6599. https://doi.org/10.1039/b905841a

540 5. Adamska-Venkatesh A, Roy S, Siebel JF, et al (2015) Spectroscopic Characterization
541 of the Bridging Amine in the Active Site of [FeFe] Hydrogenase Using Isotopologues
542 of the H-Cluster. J Am Chem Soc 137:12744–12747.
543 https://doi.org/10.1021/jacs.5b06240

544 6. Birrell JA, Pelmenschikov V, Mishra N, et al (2020) Spectroscopic and
545 Computational Evidence that [FeFe] Hydrogenases Operate Exclusively with CO-
546 Bridged Intermediates. J Am Chem Soc 142:222–232.
547 https://doi.org/10.1021/jacs.9b09745

548 7. Albracht SPJ, Roseboom W, Hatchikian EC (2006) The active site of the [FeFe]-
549 hydrogenase from Desulfovibrio desulfuricans. I. Light sensitivity and magnetic
550 hyperfine interactions as observed by electron paramagnetic resonance. J Biol
551 Inorg Chem 11:88–101. https://doi.org/10.1007/s00775-005-0039-8

552 8. Roseboom W, De Lacey AL, Fernandez VM, et al (2006) The active site of the
553 [FeFe]-hydrogenase from Desulfovibrio desulfuricans. II. Redox properties, light
554 sensitivity and CO-ligand exchange as observed by infrared spectroscopy. J Biol
555 Inorg Chem 11:102–118. https://doi.org/10.1007/s00775-005-0040-2

556 9. Birrell JA, Rodríguez-Maciá P, Reijerse EJ, et al (2021) The catalytic cycle of [FeFe]
557 hydrogenase: A tale of two sites. Coordination Chemistry Reviews 449:214191.
558 https://doi.org/10.1016/j.ccr.2021.214191

559 10. Silakov A, Kamp C, Reijerse E, et al (2009) Spectroelectrochemical Characterization
560 of the Active Site of the [FeFe] Hydrogenase HydA1 from Chlamydomonas
561 reinhardtii. Biochemistry 48:7780–7786. https://doi.org/10.1021/bi9009105

562 11. Corrigan PS, Tirsch JL, Silakov A (2020) Investigation of the Unusual Ability of the
563 [FeFe] Hydrogenase from Clostridium beijerinckii to Access an O2-Protected State.
564 J Am Chem Soc 142:12409–12419. https://doi.org/10.1021/jacs.0c04964

12. Sanchez MLK, Sommer C, Reijerse E, et al (2019) Investigating the Kinetic Competency of CrHydA1 [FeFe] Hydrogenase Intermediate States via Time-Resolved Infrared Spectroscopy. J Am Chem Soc 141:16064–16070. https://doi.org/10.1021/jacs.9b08348

13. Rodríguez-Maciá P, Galle LM, Bjornsson R, et al (2020) Caught in the Hinact: Crystal Structure and Spectroscopy Reveal a Sulfur Bound to the Active Site of an O2-stable State of [FeFe] Hydrogenase. Angewandte Chemie International Edition 59:16786–16794. https://doi.org/10.1002/anie.202005208

14. Senger M, Laun K, Wittkamp F, et al (2017) Proton-Coupled Reduction of the Catalytic [4Fe-4S] Cluster in [FeFe]-Hydrogenases. Angewandte Chemie International Edition 56:16503–16506. https://doi.org/10.1002/anie.201709910

15. Rodríguez-Maciá P, Pawlak K, Rüdiger O, et al (2017) Intercluster Redox Coupling Influences Protonation at the H-cluster in [FeFe] Hydrogenases. J Am Chem Soc 139:15122–15134. https://doi.org/10.1021/jacs.7b08193

16. Millo D, Hildebrandt P, Pandelia M-E, et al (2011) SEIRA Spectroscopy of the Electrochemical Activation of an Immobilized [NiFe] Hydrogenase under Turnover and Non-Turnover Conditions. Angewandte Chemie International Edition 50:2632–2634. https://doi.org/10.1002/anie.201006646

17. Moss D, Nabedryk E, Breton J, Mäntel W (1990) Redox-linked conformational changes in proteins detected by a combination of infrared spectroscopy and protein electrochemistry. European Journal of Biochemistry 187:565–572. https://doi.org/10.1111/j.1432-1033.1990.tb15338.x

18. Silakov A (2022) 3D Models page of the Silakov Lab website. https://sites.psu.edu/silakovlab/3d-models/. Accessed 31 Mar 2022

19. Lanz ND, Grove TL, Gogonea CB, et al (2012) Chapter Seven - RlmN and AtsB as Models for the Overproduction and Characterization of Radical SAM Proteins. In: Hopwood DA (ed) Methods in Enzymology. Academic Press, pp 125–152

20. Li H, Rauchfuss TB (2002) Iron Carbonyl Sulfides, Formaldehyde, and Amines Condense To Give the Proposed Azadithiolate Cofactor of the Fe-Only Hydrogenases. J Am Chem Soc 124:726–727. https://doi.org/10.1021/ja016964n

21. Schmidt M, Contakes SM, Rauchfuss TB (1999) First Generation Analogues of the Binuclear Site in the Fe-Only Hydrogenases: Fe2(μ-SR)2(CO)4(CN)22-. J Am Chem Soc 121:9736–9737. https://doi.org/10.1021/ja9924187

22. Seyferth D, Henderson RS, Song LC (1982) Chemistry of .mu.-dithio-bis(tricarbonyliron), a mimic of organic disulfides. 1. Formation of di-.mu.-thiolate-

bis(tricarbonyliron) dianion. Organometallics 1:125–133. https://doi.org/10.1021/om00061a022

23. Bird CL, Kuhn AT (1981) Electrochemistry of the viologens. Chem Soc Rev 10:49–82. https://doi.org/10.1039/CS9811000049

24. Silakov A (2022) Software page of the Silakov Lab website. https://sites.psu.edu/silakovlab/software/. Accessed 24 Mar 2022

25. Polcari D, Dauphin-Ducharme P, Mauzeroll J (2016) Scanning Electrochemical Microscopy: A Comprehensive Review of Experimental Parameters from 1989 to 2015. Chem Rev 116:13234–13278. https://doi.org/10.1021/acs.chemrev.6b00067

26. Rittle J, Younker JM, Green MT (2010) Cytochrome P450: The Active Oxidant and Its Spectrum. Inorg Chem 49:3610–3617. https://doi.org/10.1021/ic902062d